DOI: 10.1002/ejic.200901130

Mild Synthetic Routes to High-Surface Zinc Oxide Nanopowders

Marc Estruga,*[a] Concepción Domingo,[b] and José A. Ayllón*[a]

Keywords: Zinc / Mesoporous materials / Nanoparticles / Synthesis design / Semiconductors

ZnO nanostructured powders have been prepared at low temperature and atmospheric pressure by thermal decomposition of solid precursors. Two alternative methods have been explored by using: (i) commercial zinc acetate dihydrate and (ii) a solid mixture obtained after the evaporation of a solution of zinc acetate in aqueous ammonia at 90 °C. Powder X-ray diffraction characterization shows that in both cases crystalline ZnO was obtained after precursor treatment at 90 °C over 150 h. According to attenuated total reflection Fourier transform infrared analysis, powders obtained by both routes retain a small percentage of adsorbed acetate. Elemental analysis proves that almost 98 wt.-% of acetate was removed during the low-temperature treatment. Low-temperature nitrogen adsorption-desorption characterization shows the existence of two types of pores: intra-aggregate mesopores and interaggregate macropores. The specific surface area reached a value of 35 $m^2 g^{-1}$ for materials obtained following the direct route (i) and increased to 60 $m^2 g^{-1}$ for powders obtained by the ammonia route (ii). TEM characterization confirms the presence of a hierarchical pore structure as a result of the formation of sub-micrometric porous aggregates (50–200 nm) composed of nanocrystals smaller than 20 nm.

Introduction

Zinc oxide (ZnO) is a technologically valuable semiconductor that has attracted considerable attention because of its excellent catalytic, electrical, and optical properties.[1,2] Therefore, ZnO-based materials find numerous technological applications in solar cells, transparent conducting films, ultraviolet-protection films, chemical sensors, and light-emitting or laser diodes, among others.[3–10]

ZnO properties are notably dependent on the synthesis method employed. Hence, much effort has been dedicated to synthesize ZnO with controlled morphology and crystallite size at the micro- and nanoscale levels, because of the strong influence of these parameters on material properties. In addition, ZnO with a porous architecture is advantageous for some applications that require a high surface-to-volume ratio.[9,10] A great variety of synthetic methods have been essayed for the preparation of nanostructured ZnO powders. These include sol–gel, microemulsion, hydrothermal, spray pyrolysis, and thermal decomposition of Zn precursors, to name the most frequently used techniques.[11–22] However, most of these methods required a controlled synthesis environment, or involved the use of expensive equipment and/or high-temperature or high-pressure conditions. In this context, there is a growing interest in developing low-temperature methods for the manufacture of advanced materials such as nanostructured semiconductors. As a consequence, the direct growth of porous ZnO materials that avoids the use of templates and multistep procedures is especially relevant.

Several zinc compounds, including zinc nitrate, zinc oxalate, zinc acetylacetonate, zinc hydroxycarbonate, and zinc acetate, have been used to produce crystalline ZnO by simple thermal decomposition of solid precursors.[23–27] The described thermal processes usually work at temperatures above 300 °C,[11,24,25,28,29] although milder conditions (180 °C) could be used starting from a zinc peroxide precursor.[30,31] In some thermal decomposition processes, organic additives were added to control the size and morphology of the formed ZnO.[32]

In this work, a low-temperature thermal decomposition of zinc acetate based precursors is proposed. This process allows the preparation of a mesoporous material with a relatively high specific surface area, which is desirable for advanced ZnO applications. The method is particularly attractive for its minimal equipment requirement, low cost of chemicals, and prospective industrial-scale production.

Results and Discussion

The precursor used in the direct route, was commercial zinc acetate dihydrate (ZAD). The measured weight loss for this precursor after prolonged (150 h) thermal treatment at 90 °C in a forced-air-circulation oven suggested complete transformation of ZAD to ZnO [sample labelled as ZnO(dr)]. Moreover, XRD analysis of the ZnO(dr) sample

[a] Departamento de Química, Universidad Autónoma de Barcelona,
Campus UAB, 08193 Bellatera, Spain
Fax: +34-93581 2920
E-mail: JoseAntonio.Ayllon@uab.es
mestruga@qf.uab.cat
[b] Instituto de Ciencia de Materiales de Barcelona, CSIC,
Campus UAB, 08193 Bellaterra, Spain

(Figure 1) confirms the formation of crystalline ZnO after 150 h, all the peaks can be assigned to the hexagonal ZnO structure [JCPDS no. 79–2205]. The only intermediate detected by XRD during the transformation of ZAD into ZnO is anhydrous zinc acetate (JCPDS no. 01–0089, Figure 1). The applied low-temperature treatment precluded a mechanism for ZnO formation on the basis of the oxidation of the acetate. Alternatively, the characteristic smell of acetic acid detected during the process suggests a simple hydrolysis reaction. Thus, water vapor reacted with zinc acetate to yield acetic acid that evaporated and ZnO remained as a solid residue.[33] In addition, experiments under dry nitrogen confirm that only weight loss corresponding to the dehydration step was detected. Hence, a two-step reaction mechanism is proposed: ZAD loses its water of crystallization in the first step [Equation (1)] and anhydrous zinc acetate reacts with atmospheric water to yield zinc oxide and acetic acid [Equation (2)].

$$Zn(CH_3COO)_2{\cdot}2H_2O \rightarrow Zn(CH_3COO)_2 + 2H_2O \quad (1)$$

$$Zn(CH_3COO)_2 + H_2O \rightarrow ZnO + 2CH_3COOH \quad (2)$$

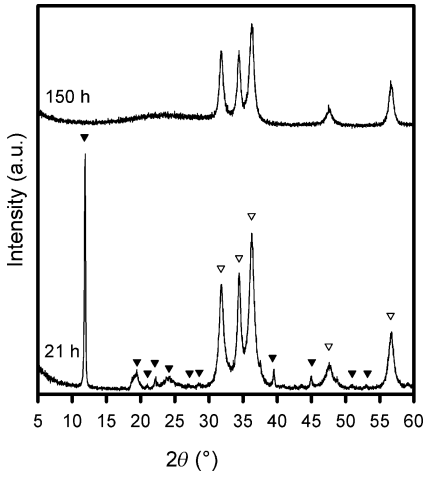

Figure 1. Powder XRD pattern of the samples obtained following the direct route at 21 h (intermediate) and 150 h [ZnO(dr)]. The pattern at 21 h shows several peaks assigned to anhydrous zinc acetate (▼, JCPDS no. 01–0089) in addition to the representative peaks of ZnO (▽, JCPDS no. 79–2205).

In the studied second route for the formation of ZnO, the precursor was produced by adding aqueous ammonia to ZAD. The pursued strategy was to convert at least a part of the acetate to ammonium acetate, a compound that starts to sublime at 53 °C.[34] However, XRD characterization reveals that the intermediate is a complex mixture of several compounds (Figure 2). In the initial stages ($t <$ 24 h) of the 90 °C treatment, part of the precursor loses its water of crystallization, as observed in the direct route, since anhydrous $Zn(CH_3COO)_2$ was detected in the mixture (peaks corresponding to this compound are marked with ▼ in the pattern recorded at 3 h in Figure 2). Later, after 24 h of treatment, the mixture evolved and anhydrous zinc acetate was no longer detected. After 48 h, broad peaks that can be assigned to ZnO appeared (▽, pattern at 48 h, Figure 2), which indicates that zinc oxide started to grow, together with a crystalline phase that has an intense peak at 9.35°. A phase with a strong peak in the same position was observed by Biswick et al. during thermal degradation of a zinc hydroxy acetate $\{Zn_5(OH)_8(CH_3CO_2)_2{\cdot}4H_2O\}$,[35] and was tentatively assigned to "$Zn_3(OH)_4(CH_3COO)_2$". This compound slowly decomposed, since it was still present as a minor component in the sample after 112 h, which is basically ZnO (Figure 2). After 150 h of thermal treatment, only ZnO was detected [sample labelled as ZnO(ar)].

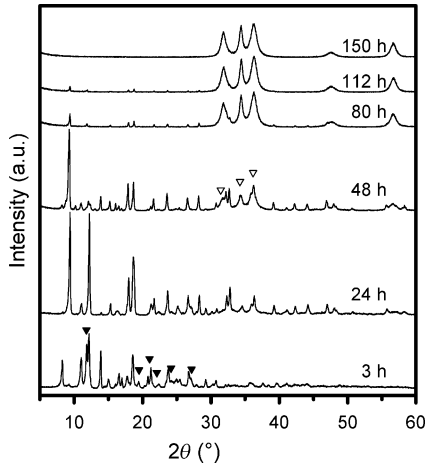

Figure 2. Powder XRD analysis of the samples obtained following the ammonia route after 3, 24, 48, 80, 112, and 150 h [ZnO(ar)]. Marked peaks correspond to anhydrous zinc acetate (▼, JCPDS no. 01–0089).

Attenuated total reflection Fourier transform infrared spectroscopy (ATR-FTIR) characterization of ZnO(dr) and ZnO(ar) (Figure 3) shows that materials prepared by both routes retain some amount of acetate adsorbed onto their surface. The peaks at 1425 and 1575 cm^{-1} are assigned to carboxylate symmetric and antisymmetric stretches, respectively, of the acetate molecule. Moreover, the position of these peaks indicate that acetate is attached to the ZnO surface as a monodentate ligand.[36,37] The stretching vibration mode of the CH_3 group can also be detected at 2930 cm^{-1}. Furthermore, the incorporation of acetate was quantified by elemental analysis (1.50 and 3.50 wt.-% for the direct and ammonia routes, respectively). Hence, ca. 98–99 wt.-% of initial acetate was removed at the end of the processes. Acetate removal during the synthesis procedure is higher for the direct route than when ammonia was employed.

The weight loss of the samples, determined by TG analysis (Figure 4), confirms that the amount of acetate and water in the prepared powders is in the order of 3–4 wt.-%. The gradual removal of acetate was observed in the 300–500 °C range. This fact differs from previously obtained results on thermal decomposition of ZAD, in which no weight loss was detected beyond 300–380 °C.[11,29,32,33,38,39] Consequently, it could be concluded that the remaining acetate after ZnO synthesis is strongly coordinated to the powder surface, since it requires higher temperatures to be eliminated.

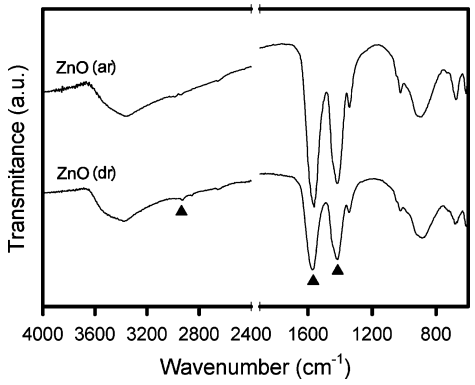

Figure 3. ATR-FTIR characterization of samples ZnO(dr) and ZnO(ar). Marked peaks at 1425, 1575, and 2930 cm^{-1} correspond to vibrations of residual acetate.

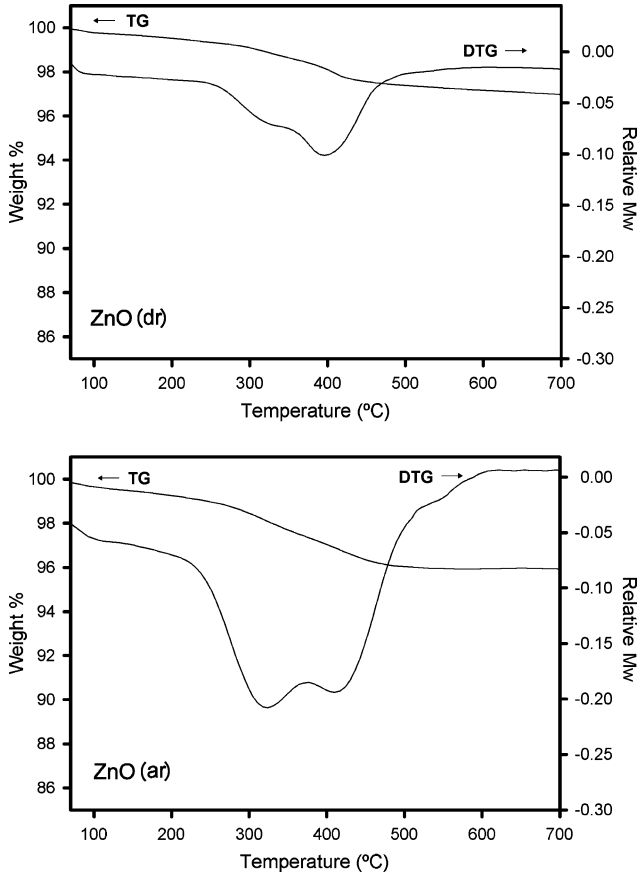

Figure 4. Thermogravimetric analysis of the of samples ZnO(dr) and ZnO(ar).

Low-temperature nitrogen adsorption–desorption analysis shows that materials obtained by both routes have similar textural characteristics (Figure 5a). Recorded isotherms are of type II and present two hysteresis loops, which indicates a bimodal porosity. At relative pressures between 0.4 and 0.8, the hysteresis loop is of type H2, which suggests the presence of intra-aggregate pores with an ink-bottle morphology, whereas between 0.8 and 1.0, it is of type H3, which could be associated with the formation of interaggregate macropores.[40–42] The pore size distribution (Figure 5b), calculated from the adsorption branch,[43] denotes the presence of mesopores in the 25–100 Å range, which is related to the H2 hysteresis loop. The presence of ammonia in the precursor induces a reduction in the pore diameter (about 25%) (Figure 5b). For the ZnO(dr) sample, the estimated specific surface area (S_a) is 37 $m^2 g^{-1}$, which increases to 60 $m^2 g^{-1}$ for the ZnO(ar) sample. The high S_a value for the ZnO(ar) powder is related to the reduction in the pore diameter, as well as to the increased amount of residual acetate, which acts as a capping agent and minimizes powder agglomeration. The estimated S_a values are relatively large, in comparison with those reported for ZnO powders prepared following other high-temperature processes. For example, the thermal decomposition of zinc acetate at 400 °C leads to the formation of ZnO powders with an S_a value of 6 $m^2 g^{-1}$, and this value decreases by increasing the treatment temperature.[26] Unfortunately, in numerous studies related to the synthesis of ZnO by thermal decomposition, the specific surface area of the prepared samples has not been determined. In addition, most industrial-scale production methods of ZnO nanopowders are performed by oxidation of Zn vapors, which gives S_a values of ca. 18–25 $m^2 g^{-1}$.[44]

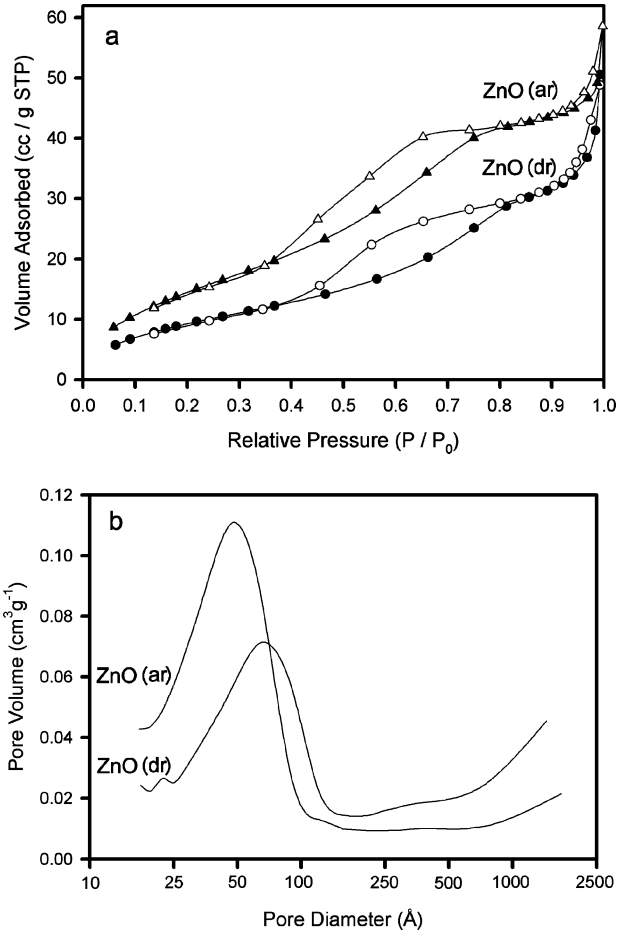

Figure 5. Low-temperature nitrogen adsorption–desorption characterization of samples ZnO(dr) and ZnO(ar): (a) isotherms and (b) pore size distribution estimated by using the adsorption branch of the isotherm.

The ZnO materials prepared by both studied routes show a high absorption capacity of UV-A radiation and complete transparency in the visible region, according to UV/Vis diffuse reflectance spectroscopy (UV/Vis DRS) analysis (Figure 6). A band gap value of 3.2 eV was estimated for both prepared ZnO powders after 150 h. This value indicates that the crystallite size is bigger than the quantization limit (7 nm).[45]

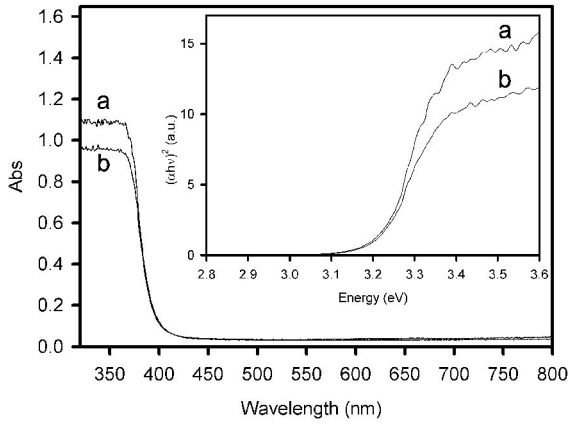

Figure 6. UV/Vis diffuse reflectance absorption spectra of the (a) ZnO(dr) and (b) ZnO(ar) materials. Inset: a plot of the transformed Kubelka–Munk function vs. the energy of absorbed light.

SAED analysis of ZnO(dr) and ZnO(ar) shows a ring pattern with discrete bright spots and interplanar distances associated with the most intense rings (2.78, 2.57, and 2.45 Å), which confirms that ZnO is the only crystalline phase (data not shown). TEM characterization shows that both materials, ZnO(dr) (Figure 7a, c, e) and ZnO(ar) (Figure 7b, d, f), contain nanocrystals smaller than 20 nm that aggregate to form secondary particles of ca. 50–200 nm, which indicates the porous nature of the material. This specific arrangement is likely to be responsible for the hierarchical bimodal pore structure, which includes intra-aggregate mesopores and interaggregate macropores. HRTEM (insets of Figure 7e, f) confirms the crystalline nature of the nanoparticles. In addition, for both routes, the aggregates are quite transparent in the low-magnification micrographs, which indicates that the electron beam could cross the whole aggregate. This fact suggests that the aggregates have a roughly flat shape. In the ZnO(ar) micrographs (Figure 6b, d, f), the aggregates have a more defined geometry, and the primary particles are slightly smaller and have a more regular size than those obtained by the direct route. This could be related to the different intermediates detected in both routes, as well as to the higher acetate content for the ZnO(ar) sample, which limits crystal growth to a higher extent.

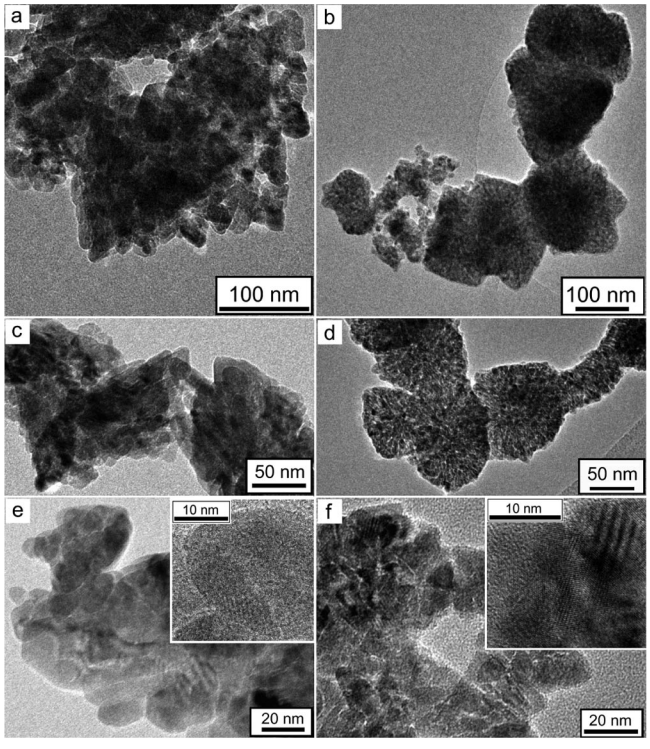

Figure 7. TEM micrographs of samples: (a, c, e) ZnO(dr) and (b, d, f) ZnO(ar). HRTEM micrographs included (insets of e and f).

Conclusions

Nanocrystalline wurtzite ZnO was obtained by thermal decomposition of two different precursors at 90 °C for 150 h: (i) a commercial zinc acetate dihydrate and (ii) a solid mixture obtained after evaporation of a solution of zinc acetate in aqueous ammonia. Elemental analysis reveals that almost 98 wt.-% of the initial acetate was removed during the applied low-temperature decomposition treatment. TEM characterization and N_2 sorption analysis indicate that nanocrystals smaller than 20 nm grow and assemble (probably at the same time) to form aggregates of 50–200 nm with a bimodal porosity; they include ink-bottle intra-aggregate mesopores and slitlike interaggregate macropores. The residual acetate is strongly attached to the powder surface, and thus minimizes the agglomeration, which leads to high specific surface area values for the obtained ZnO materials. The ammonia route leads to materials with higher surface areas. The main advantage of the reported methods is their simplicity; no special equipment or chemical reagents are required and the use of organic solvents is excluded. The proposed method completely avoids contamination with alkaline metals, which is common in several methods for the synthesis of ZnO. Moreover, the used acetate is not oxidized and, thus, can be recovered.

Experimental Section

Reagents: Both zinc acetate dihydrate $\{Zn(CH_3COO)_2{\cdot}2H_2O\}$ and aqueous ammonia were of reagent grade (Aldrich) and used without further purification. Ultrapure doubly distilled and deionized water (Milli-Q system, conductivity lower than 0.05 μS/cm) were employed.

Synthesis

Direct Route: ZAD (1.22 g, 5.57 mmol) was spread on a Petri dish (12 cm in diameter) and heated at 90 °C in a conventional oven

with forced ventilation. The evolution of the sample was followed gravimetric and by X-ray diffraction characterization. After 150 h of treatment, it was observed that the sample weight remained stable and the powder XRD pattern only contained ZnO peaks. The sample at 150 h was labelled as ZnO(dr).

Ammonia Route: ZAD (1.22 g, 5.57 mmol) was dissolved in concentrated aqueous ammonia (10 mL, 71 mmol). In this step, precipitation of zinc hydroxide and its further dissolution were both observed. The solution was then transferred to a Petri dish and evaporated at 90 °C in a hot plate. After solvent evaporation, the Petri dish containing the residue was introduced into an oven maintained at 90 °C with forced ventilation. The evolution of the samples was monitored as in the former route. Thermal treatment was maintained for 150 h to obtain ZnO. The sample was labelled as ZnO(ar).

Characterization: Gravimetric analysis was carried out with a Sartorius BP 110 S precision balance. XRD spectra of powder samples were registered on a Rigaku Rotaflex RU-200B diffractometer by using Cu-$K_{\alpha 1}$ radiation (λ = 1.5406 Å). Electron diffraction patterns and TEM and HRTEM images were recorded with a JEOL 2011 microscope operating at 200 kV. The acquired images were analyzed with a Gatan Digital Micrograph (software version 3.10.0). ATR-FTIR spectra were recorded with a Bruker apparatus (Tensor model, equipped with a MKII Golden Gate). TGA was performed with a TGA7 instrument from Perkin–Elmer. Textural characteristics of the obtained and commercial ZnO nanopowder were studied by low-temperature N_2 adsorption–desorption analysis (ASAP 2000 Micromeritics). Prior to measurements, the samples were dried under reduced pressure (<1 mPa) at 393 K for 18 h. The specific surface area was determined by the BET method.[46] The mean pore diameter was estimated by using the BJH method.[47] A Perkin–Elmer Lambda 19 UV/Vis/NIR spectrophotometer, furnished with a 60-mm integrating sphere, was used for UV/Vis diffuse reflectance spectroscopy measurements on solid samples, with $BaSO_4$ as the reference. Spectra were recorded in the diffuse reflectance mode and transformed to a magnitude proportional to the extinction coefficient through the Kubelka–Munk function. Elemental analysis was performed by using a 3011 CHNS analyzer (EuroVector).

Acknowledgments

The work described in this paper was supported by the Spanish National Plan of Research (projects CTQ2005-02808/PPQ and CTQ2008-00178). The authors wish to thank Dr. Xavier Saurina (Universitat de Barcelona) for assistance with the UV/Vis DRS characterization and Dr. Emma Rossinyol (Servei de Microscopia UAB) for helpful discussions on TEM.

[1] Z. Y. Fan, J. G. Lu, *J. Nanosci. Nanotechnol.* **2005**, *5*, 1561–1573.
[2] S. J. Pearton, D. P. Norton, K. Ip, Y. W. Heo, T. Steiner, *Prog. Mater. Sci.* **2005**, *50*, 293–340.
[3] M. C. Carotta, A. Cervi, V. di Natale, S. Gherardi, A. Giberti, V. Guidi, D. Puzzovio, B. Vendemiati, G. Martinelli, M. Sacerdoti, D. Calestani, A. Zappettini, M. Zha, L. Zanotti, *Sens. Actuators B* **2009**, *137*, 164–169.
[4] E. Guillen, C. Fernandez-Lorenzo, R. Alcantara, J. Martin-Calleja, J. A. Anta, *Sol. Energy Mater.* **2009**, *93*, 1846–1852.
[5] A. Moustaghfir, E. Tomasella, A. Rivaton, B. Mailhot, M. Jacquet, J. L. Gardette, J. Cellier, *Surf. Coat. Technol.* **2004**, *180–81*, 642–645.
[6] T. Minami, *Thin Solid Films* **2008**, *516*, 5822–5828.
[7] X. M. Zhang, M. Y. Lu, Y. Zhang, L. J. Chen, Z. L. Wang, *Adv. Mater.* **2009**, *21*, 2767–2770.
[8] S. Chu, M. Olmedo, Z. Yang, J. Y. Kong, J. L. Liu, *Appl. Phys. Lett.* **2008**, *93*, 181106.
[9] J. Zhang, S. R. Wang, M. J. Xu, Y. Wang, B. L. Zhu, S. M. Zhang, W. P. Huang, S. H. Wu, *Cryst. Growth Des.* **2009**, *9*, 3532–3537.
[10] F. Lu, W. P. Cai, Y. G. Zhang, *Adv. Funct. Mater.* **2008**, *18*, 1047–1056.
[11] S. Labuayai, V. Promarak, S. Maensiri, *Appl. Phys. A: Mater.* **2009**, *94*, 755–761.
[12] H. Van den Rul, D. Mondelaers, M. K. Van Bael, J. Mullens, *J. Sol-Gel Sci. Technol.* **2006**, *39*, 41–47.
[13] V. Ischenko, S. Polarz, D. Grote, V. Stavarache, K. Fink, M. Driess, *Adv. Funct. Mater.* **2005**, *15*, 1945–1954.
[14] G. W. Xiong, L. T. Luo, C. Q. Li, X. M. Yang, *Energy Fuels* **2009**, *23*, 1342–1346.
[15] W. L. Suchanek, *J. Cryst. Growth* **2009**, *312*, 100–108.
[16] M. J. Height, L. Madler, S. E. Pratsinis, F. Krumeich, *Chem. Mater.* **2006**, *18*, 572–578.
[17] J. Zhang, L. D. Sun, X. C. Jiang, C. S. Liao, C. H. Yan, *Cryst. Growth Des.* **2004**, *4*, 309–313.
[18] K. C. Barick, M. Aslam, V. P. Dravid, D. Bahadur, *J. Phys. Chem. C* **2008**, *112*, 15163–15170.
[19] S. Bhattacharyya, A. Gedanken, *Microporous Mesoporous Mater.* **2008**, *110*, 553–559.
[20] D. Domide, E. Kaifer, J. Mautz, O. Walter, S. Behrens, H. J. Himmel, *Eur. J. Inorg. Chem.* **2008**, 3177–3185.
[21] J. Y. Li, H. Y. Peng, J. Liu, H. O. Everitt, *Eur. J. Inorg. Chem.* **2008**, 3172–3176.
[22] M. Starowicz, B. Stypula, *Eur. J. Inorg. Chem.* **2008**, 869–872.
[23] C. C. Lin, Y. Y. Li, *Mater. Chem. Phys.* **2009**, *113*, 334–337.
[24] L. Guo, Y. L. Ji, H. B. Xu, Z. Y. Wu, P. Simon, *J. Mater. Chem.* **2003**, *13*, 754–757.
[25] C. Shifu, Z. Wei, Z. Sujuan, L. Wei, *Chem. Eng. J.* **2009**, *148*, 263–269.
[26] N. Audebrand, J. P. Auffredic, D. Louer, *Chem. Mater.* **1998**, *10*, 2450–2461.
[27] G. A. M. Hussien, *Thermochim. Acta* **1991**, *186*, 187–197.
[28] L. M. Shen, L. C. Guo, N. Z. Bao, K. Yanagisawa, *Chem. Lett.* **2003**, *32*, 826–827.
[29] X. Y. Zhao, B. C. Zheng, C. Z. Li, H. C. Gu, *Powder Technol.* **1998**, *100*, 20–23.
[30] Y. C. Zhang, X. Wu, X. Y. Hu, R. Guo, *J. Cryst. Growth* **2005**, *280*, 250–254.
[31] S. Cheng, D. Yan, J. T. Chen, R. F. Zhuo, J. J. Feng, H. J. Li, H. T. Feng, P. X. Yan, *J. Phys. Chem. C* **2009**, *113*, 13630–13635.
[32] Y. Yang, H. L. Chen, B. Zhao, X. M. Bao, *J. Cryst. Growth* **2004**, *263*, 447–453.
[33] T. Arii, A. Kishi, *Thermochim. Acta* **2003**, *400*, 175–185.
[34] M. Olszak-Humienik, *Thermochim. Acta* **2001**, *378*, 107–112.
[35] T. Biswick, W. Jones, A. Pacula, E. Serwicka, J. Podobinski, *Solid State Sci.* **2009**, *11*, 330–335.
[36] T. Ishioka, Y. Shibata, M. Takahashi, I. Kanesaka, Y. Kitagawa, K. T. Nakamura, *Spectrochim. Acta A* **1998**, *54*, 1827–1835.
[37] S. Sakohara, M. Ishida, M. A. Anderson, *J. Phys. Chem. B* **1998**, *102*, 10169–10175.
[38] A. V. Ghule, K. Ghule, C. Y. Chen, W. Y. Chen, S. H. Tzing, H. Chang, Y. C. Ling, *J. Mass Spectrom.* **2004**, *39*, 1202–1208.
[39] A. V. Ghule, B. Lo, S. H. Tzing, K. Ghule, H. Chang, Y. C. Ling, *Chem. Phys. Lett.* **2003**, *381*, 262–270.
[40] K. S. W. Sing, D. H. Everett, R. A. W. Haul, L. Moscou, R. A. Pierotti, J. Rouquerol, T. Siemieniewska, *Pure Appl. Chem.* **1985**, *57*, 603–619.
[41] W. Ho, J. C. Yu, S. Lee, *Chem. Commun.* **2006**, 1115–1117.
[42] J. G. Yu, J. C. Yu, W. K. Ho, M. K. P. Leung, B. Cheng, G. K. Zhang, X. J. Zhao, *Appl. Catal. A* **2003**, *255*, 309–320.

[43] J. C. Groen, L. A. A. Peffer, J. Perez-Ramirez, *Microporous Mesoporous Mater.* **2003**, *60*, 1–17.
[44] S. Kaluza, M. K. Schroter, R. N. d'Alnoncourt, T. Reinecke, M. Muhler, *Adv. Funct. Mater.* **2008**, *18*, 3670–3677.
[45] E. A. Meulenkamp, *J. Phys. Chem. B* **1998**, *102*, 5566–5572.
[46] S. Brunauer, P. H. Emmett, E. Teller, *J. Am. Chem. Soc.* **1938**, *60*, 309–319.
[47] E. P. Barrett, L. G. Joyner, P. P. Halenda, *J. Am. Chem. Soc.* **1951**, *73*, 373–380.

Received: November 20, 2009
Published Online: March 1, 2010

